Journal of
Computer Science & Systems Biology

Peng et al., J Comput Sci Syst Biol 2015, 8:3
DOI: 10.4172/jcsb.1000186

Research Article Open Access

Efficient Image Resolution Enhancement Using Edge-Directed Unsharp Masking Sharpening for Real-Time ASIC Applications

Kuo-Shiuan Peng[1], Fang-Cheng Lin[2]* and Kai-Tung Teng[2]

[1]*Department of Electronic and Computer Science, University of Arizona, 1230 E. Speedway Blvd. P.O. Box 210104 Tucson, AZ 85721-0104, USA*
[2]*Department of Photonics and Display Institute, National Chiao Tung University, 30010 Hsinchu, Taiwan*

Abstract

This paper proposes the edge-directed unsharp masking sharpening (EDUMS) method and demonstrates the method's ability to provide single-image resolution enhancement. The EDUMS method implements an efficient single-image, super-resolution process by synergizing edge-directed information and unsharp masking sharpening. This study designs a simple and robust edge information detection process for unsharp masking sharpening that is used to produce a clear edge structure and vivid details of high-resolution images with minimal ringing and jaggy artifacts. This method is a non-iterative process that is computationally efficient for use in a real-time integrated circuit design implementation.

Keywords: Directed edge; Image resolution enhancement; Super resolution; Unsharp masking sharpening

Introduction

Recently, the resolution of flat panel displays has substantially increased from WXGA resolution (1366×7 68 pixels) to UHD resolution (3840 × 2160 pixels). However, the resolutions of most broadcasting content remain in SD (720 × 480 pixels) or HD (1280 × 720 pixels); limited sources exist in FHD (1920 × 1080 pixels), and UHD is rare [1,2]. Therefore, resolution enhancement in video chip applications has attracted substantial attention. A practical implementation for expanding images consists of linear or bicubic interpolation. These methods efficiently increase content pixel resolution; however, these methods also decrease image sharpness due to a loss of edge and detail information. Therefore, an appropriate method for restoring image quality when expanding images by enhancing high-frequency structures must be developed.

In the computer vision field, single-image, super-resolution (SR) technology has been extensively studied [3,4], the iterative and unsharp masking sharpening (UMS) are the two main approaches. The iterative methods include example based multi-resolution SR [3-9] which construct the SR image by learning to different types of training set, Gaussian process regression [10] which use covariance function through the Gaussian process regression to reconstruct the SR image, sparse representation model [11-14] which use the sparse representation model of compressed sensing to recover the SR image, and back projection [15,16] which has the concept of iteratively back projecting the difference between estimated SR image and simulated low-resolution images. Those methods succeed in upscaling vivid SR images, but requiring the iteration process or a training processing and hindering the use of these methods in practical IC designs.

On the other hand, a popular method used in video applications is filtering sharpening using the unsharp masking method [17-21]. Previous studies using this method have produced simple yet important results with enhanced details, which are more potential to be implemented in real-time applications; however, the edge structure may be distorted due to jaggy and ringing artifacts [22], as shown in Figure 1, which prompt the consideration of edge-preserving sharpening techniques [23,24]. However, when the edge structure is preserved, the details in a high-frequency area become flat and may disappear. The filtering sharpening process has limitations in terms of the balance between edge structure reconstruction and detail enhancement.

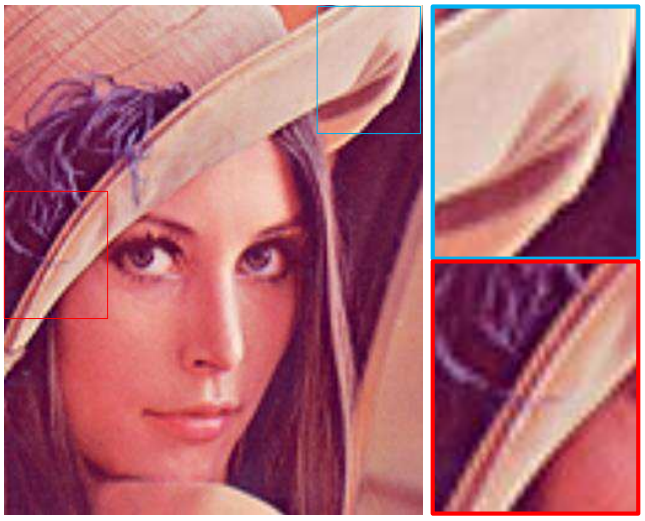

Figure 1: (a) 3X resolution enhancement using the conventional unsharp masking sharpening and (b) magnified images with ringing and jaggy artifacts.

To address edge reconstruction problems, edge-directed SR techniques have become very popular over the past decade. Gradient detection algorithms are often used to determine edge information in studies on edge reconstruction. A common method is the directional, filter-based [25-27] image enhancement. For example, contourlet-based [28] sharpening can provide eight directional filters that can be used to calculate edge information. Incorporating gradient prior methods,

***Corresponding author:** Fang-Cheng Lin, Department of Photonics and Display Institute, National Chiao Tung University, 30010 Hsinchu, Taiwan, Tel: 03-5712121 turn 59353; Fax: 03-5737681; Email: fclin.eo93g@nctu.edu.tw

Received April 24, 2015; **Accepted** May 13, 2015; **Published** May 15, 2015

Citation: Peng KS, Lin FC, Teng KT (2015) Efficient Image Resolution Enhancement Using Edge-Directed Unsharp Masking Sharpening for Real-Time ASIC Applications. J Comput Sci Syst Biol 8: 174-184. doi:10.4172/jcsb.1000186

additionally, recently developed edge-directed SR methods [29-34] can recover or simulate the edge structure from a low-resolution source image or a reference image. However, the preparation of the edge-directed information in those methods is computationally complex; thus, these methods are not practical in ASIC applications.

In summary, using iterative methods can reconstruct high image quality but take too much time and cost due to high computational complexity. In contrast, UMS-related methods face the jaggy and ringing artifacts or detail information lost even though these methods are promising for real-time practical ASIC applications. As a result, this paper develops a real-time, single-image, super-resolution method by synergizing unsharp masking sharpening and edge-directed priors with a novel edge detection method. The basic concept is derived from the efficiency of unsharp masking sharpening [17,18,20] and the clear edge structure representation from edge-directed priors [25,28,30]. This study decomposes the edge information for unsharp masking sharpening to resolve jaggy, ringing artifacts that result from the filtering sharpening processes and to improve the computational efficiency of the directional information processes.

Algorithm Flowchart

This paper reviews the basis of the conventional unsharp masking sharpening (conventional UMS) [17-24] process. This process can be modeled with the following equations:

$$I_{cums\_dlt} = Sx * I_{x+i} + Sy * I_{y+j} \quad (1)$$

$$I_{cums} = I + I_{cums\_dlt}$$

$$let\ i, j = -k \sim k$$

where I_{cums_dlt} is the conventional UMS processed delta; I_{cums} is the sharpened result; I_{x+i} and I_{y+j} denote neighboring data around the current data I in both the horizontal direction and the vertical direction, respectively, in range k; and Sx and Sy represent the conventional UMS operators in the horizontal direction and the vertical direction, respectively. In this paper, the symbol * represents convolution. The basic consideration was to separately enhance the horizontal and vertical gradients and obtain the sum of all enhancement values. The commonly used sharpening operators, i.e., Sx and Sy, are [-1, 2, -1], $[-1, 2, -1]^T$ and [-1, 0, 2, 0, -1], $[-1, 0, 2, 0, -1]^T$, respectively, which are second-order, differential-based filters for different frequency bandwidths. These filters were effective and easily implemented in the conventional UMS; however, substantial aliasing and a lack of directional process produced ringing issues and pronounced jaggy [22], as shown in Figures 1 and 2b. The original image profile in Figure 2a is smooth, after using the conventional UMS, the edge part is distorted with ringing and jaggy artifacts, as shown in Figure 2b, which deteriorated the image quality and fidelity. Figure 2c shows the edge information of the proposed EDUMS method, the edge clarity is enhanced compared to the original image, and further resolved the ringing and jaggy issues in conventional unsharp masking sharpening.

To address the aforementioned artifacts, this paper proposes the EDUMS method, and the algorithm process flow is shown in Figure 3. The original low-resolution (LR) image in Figure 3a is the only input. EDUMS attempts to produce the high-resolution (HR) image shown in Figure 3f while preserving edge clarity and strengthening the contrast of the details of the original LR image.

The EDUMS kernel contains two parts. First, the unsharp masking sharpening method [17] was used as the basic component of the edge and detail enhancement in Figures 3d and 3e. The unsharp masking filters of the enhancement consist of a horizontal filter and a vertical filter. The most significant improvement of this algorithm is to introduce the edge-directed prior to address ringing and jaggy issues found in the conventional UMS method. The second kernel consists of the edge structure detection function, which is based on the Canny edge detection method [34]. This step provides the edge-directed information that is represented in Figure 3c, including edge direction and intensity. A unique feature of the EDUMS approach is that this edge information can be used to control edge sharpening without ringing and jaggy issues and to adaptively determine the strength between the edge and the details in the fusion function represented in Figure 3f. These details are illustrated in the following section.

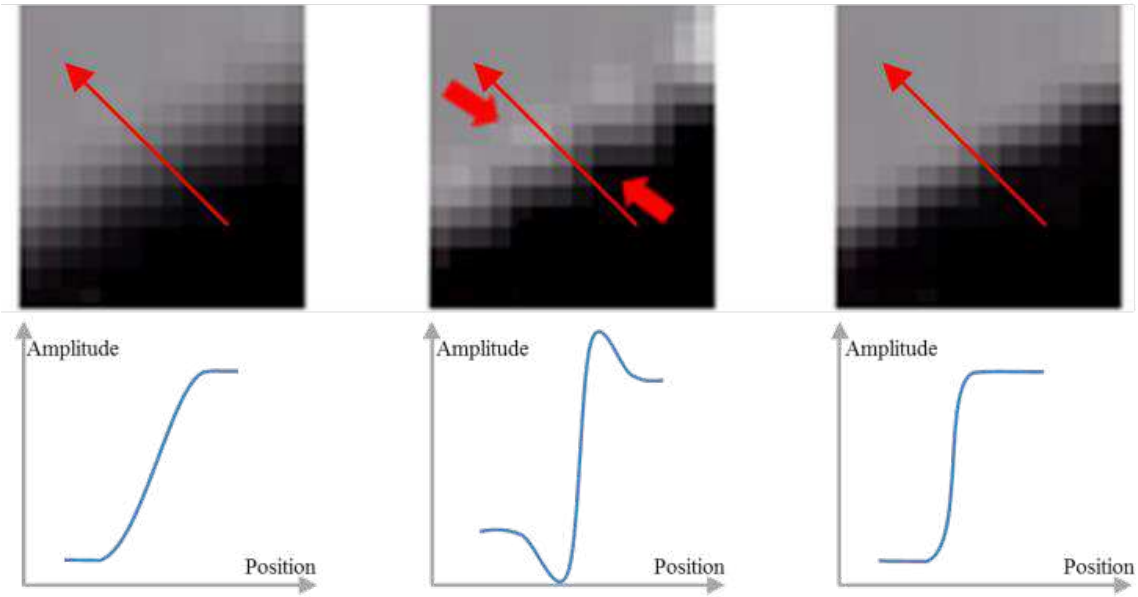

Figure 2: Edge information of (a) Source image. Images simulated using (b) conventional unsharp masking sharpening with substantial ringing and jaggy issues and (c) the proposed EDUMS method.

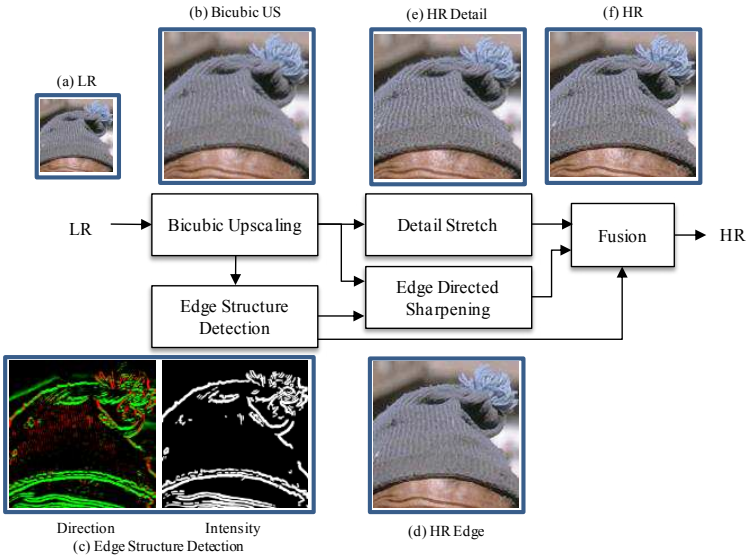

Figure 3: The flow of the proposed EDUMS method. (a) The LR image is the input for the bicubic upscaling process. (b) The bicubic upscaling (bicubic US) image is generated. (c) The edge detection function provides the edge-directed information from the bicubic US image. The direction images contain direction and intensity information. (d) Edge-directed sharpening produces the HR edge image. (e) The detail stretch component extracts the HR detail image. (f) The HR output is the fusion of the HR edge and the HR detail images.

Edge-Directed Unsharp Masking Sharpening

Transient improvement has been the premise of various studies on determining the clear edge of an image [23-32]. The gradient prior [27-32] has been extensively adopted to improve the transient along the gradient direction. This method can effectively enhance the edge transient without producing jaggy issues.

However, these methods are computationally complex and expensive. When the gradient information does not correspond to the edge profile, the directional data are not sufficient for enhancing the image resolution. The complexity of the directional data preparation and the robustness of the directional information are critical to efficiently and correctly enhancing the edge transient.

To efficiently achieve image resolution enhancement without producing jaggy and ringing artifacts, EDUMS precisely redefines the edge direction and intensity from the edge information using a Sobel operator. Edge structure detection, ringing and jaggy suppression, and the fusion method are subsequently addressed.

Edge structure detection

Canny edge detection provides stable information about an edge structure [35]. However, this information is abundant and redundant. EDUMS modifies the Canny edge detection method to ensure its suitability for the conventional UMS process. In the Canny edge detection method, the edge detection operators in the horizontal (x) and vertical (y) directions were set as Sobel operators, i.e., *Sbx=[-1, 0, 1;-2, 0, 2;-1, 0, 1]/8* and *Sby=[1, 2, 1;0, 0, 0;-1, -2, -1]/8*, respectively. The edge direction of conventional UMS using conventional Canny edge detection, the image gradients of the x and y axes, were denoted as $Gx=Sbx*I$ and $Gy=Sby*I$, respectively. The gradient direction using conventional UMS was defined as $d=Gy/Gx$, while the gradient magnitude was defined as $m=|Gx|+|Gy|$. Although the edge raw data of the conventional gradient, i.e., *E(d, m)*, are intuitive in the conventional UMS method, *E(d, m)* is not an efficient index for edge-directed information because the gradient direction *d* falls between negative infinity and positive infinity, while edge direction is constrained to the vertical direction.

An efficient method for describing the edge direction is to describe the horizontal and vertical components with a ratio. Consequently, this study decomposed the conventional edge information *E(d, m)* into normalized component edge information $E_{nc}(Edx, Ei)$ (Figure 4), which can describe edges in the normalized component aspects. To precisely and efficiently describe the edge direction, this study normalized the horizontal gradient *Gx* and the vertical gradient *Gy* using their absolute sum and decomposed the gradient direction *d* into the edge directions x and y as *Edx* and *Edy*:

$$Edx = \frac{|Gx|}{|Gx|+|Gy|}, \quad Edy = \frac{|Gy|}{|Gx|+|Gy|} = 1 - Edx, \tag{2}$$

where *Edx* and *Edy* are the horizontal and vertical direction percentages, respectively, of the gradient direction *d*. Therefore, the gradient direction *d* was simply expressed by *Edx*, which is called the component gradient direction (CGD) and falls between 0 and 1. For the case of $|Gx|+|Gy|=0$, *Edx* was set to 0 in this study.

To maintain edge continuity in a noise or weak boundary case, this study defines the edge intensity *Ei* using the following equation:

$$Ei = Eif(m, Ei_{cor}, Ei_{th})$$
$$as \quad Eif: \begin{cases} Ei = 0, m \le Ei_{cor} \\ Ei = \dfrac{(m - Ei_{cor})}{(Ei_{th} - Ei_{cor})}, Ei_{cor} < m < Ei_{th} \\ Ei = 1, m \ge Ei_{th} \end{cases} \tag{3}$$

where *Ei* is the edge intensity, which is remapped to [0, 1] using the edge intensity transfer function $Eif(m, Ei_{cor}, Ei_{th})$; Ei_{cor} is the coring value for the lower threshold; and Ei_{th} is the limit value for the upper threshold. In this step, a weak gradient in Ei_{cor} can be removed, and the intensity can be determined according to the relationship between Ei_{cor} and Ei_{th}.

Ringing and jaggy suppression

After precisely detecting the edges and their intensities, this study

suppressed the artifacts of conventional UMS, i.e., edge ringing and jaggy. The ringing issue can be addressed using a common clipping process, which is expressed as follows:

$$I_{cl}(I) = \begin{cases} Imax & , for\ I(x,y) > Imax \\ Imin & , for\ I(x,y) < Imim \\ I & , for\ other\ case \end{cases} \quad (4)$$

$$let\ I = I(x,y),$$

$$Imax = max(I(x+i, y+j)), Imin = min(I(x+i, y+j))$$

$$i, j = -k \sim k, i, j \neq 0$$

where $I_{cl}(I)$ is the clipping result of the current pixel I, $Imax$ and $Imin$ are obtained from the surrounding pixel $I(x+i,y+j)$, and the reference range is represented by k, which is generally set to one. However, this clipping process is applied to all of the pixels of the input image. So the image details are suppressed at the same time. The edge becomes clear, while the details become blurred, as shown in Figure 5c.

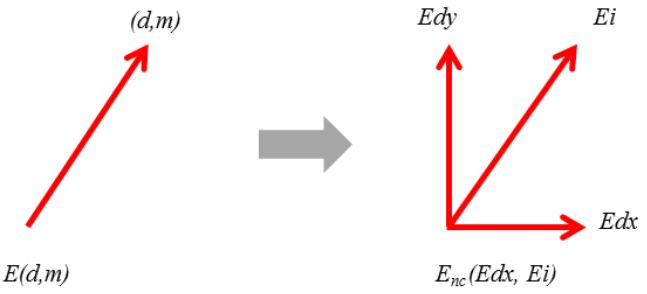

Figure 4: The conventional gradient *E(d, m)* is transferred into the normalized component edge information E_{nc} *(Edx, Ei)* using EDUMS.

In contrast, the clipping process was therefore adopted only for the edge area while using EDUMS. For the continuity of clipping, this study introduced the edge area intensity *Eai* into the clipping process as follows:

$$I_{eicl}(I_s) = \begin{cases} I_s + (Imax - I_s) \times Eai & , for\ I_s > Imax \\ I_s + (Imin - I_s) \times Eai & , for\ I_s < Imim \\ I_s & , for\ other\ case \end{cases} \quad (5)$$

$$Eai(x,y) = max(Ei(x+i, y+j)),\ i, j = -1 \sim 1$$

$$let\ I_s = sharpened\ (I(x,y))$$

$$Imax = max(I_{bc}(x+i, y+j)), Imin = min(I_{bc}(x+i, y+j))$$

$$i, j = -k\ \sim\ k,\ i, j \neq 0$$

where $I_{eicl}(I_s)$ is the edge intensity-based clipping result of the current pixel being sharpened (I_s), *Eai* is the edge area intensity, and I_{bc} is the bicubic-upscaled source image data. The edge-directed clipping method preserves the details according to the edge area intensity. A vivid image without the peaking effect is shown in Figure 5d.

After suppressing the ringing effects, the image jaggy can be detected around the edge. Two types of image jaggy exist. Source jaggy exists in the source image, whereas artificial jaggy is a result of

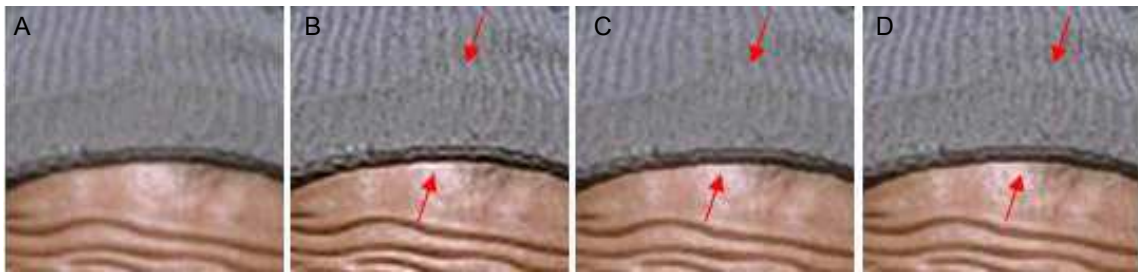

Figure 5: (a) Source image. (b) Conventional UMS without clipping process. The ringing effect occurs around the edges of the cap. (c) Conventional UMS with clipping process. The edges exhibit no ringing; however, the details become blurred. (d) The proposed EDUMS suppresses the ringing and maintains the details.

Figure 6: (a) Source image with bicubic upscaling. (b) Conventional UMS without AAF process. The jaggy effect occurs for different line angles. (c) Conventional UMS with AAF process. The jaggy effect is suppressed while the image details are blurred. (d) Proposed EDUMS with EIAAF. The AAF process is only applied to the edge area, so the edges remain smooth, and details become clear.

the enhancement process. This study considered the source jaggy to be the pre-process of the edge enhancement prior to the sharpening process. Then, this study addressed the problem of artificial jaggy in the conventional UMS method.

The source jaggy from the discontinuity along the edges may consist of intrinsic data or may be caused by the upscaling process. This study resolved one-pixel source jaggy in the upscaling image I_{bc} (bicubic US). A commonly used solution is the use of an anti-aliasing filter (*AAF*) for the entire image [30]. This approach is sufficient for resolving the jaggy issue while simultaneously suppressing the image details because the process is applied to all of the pixels of the input image (Figure 6c). Therefore, this study only applied the AAF to the edge area that was determined using the edge intensity *Ei*, which is called the edge intensity-based AAF (EIAAF). The process is expressed as follows:

$$I_{eiaaf}(I_{bc}) = Ei \times AAF * I_{bc} + (1\text{-}Ei) \times I_{bc} \qquad (6)$$

where I_{eiaaf} is the synthesized result of the bicubic-upscaled pixel I_{bc} being applied AAF. The synthesizing weighting is determined by the edge intensity *Ei,* which means the AAF is only applied to the edge part. This EIAAF method is simple and maintains high-frequency details. The performance of this preprocess is important and can be demonstrated via a comparison of Figure. 6b-6d. The details of the upper spots are well maintained using this EIAAF technique.

After resolving the source jaggy issue, the artificial jaggy that employs conventional UMS is derived from the lack of a directional process, which can be used to determine the horizontal and vertical enhancement ratio. According to Edge structure detection, this study decomposed the conventional edge information *E(d, m)* into the normalized component edge information $E_{nc}(Edx, Ei)$. With this normalized information, the edge improvement process used only horizontal and vertical directional data from its component edge information in the enhancement process. The EDUMS is then modeled as follows:

$$\begin{aligned} I_{edums\_dlt} &= Edx \times (Sx_{ums} * Ix_{eiaaf}) + Edy \times (Sy_{ums} * Iy_{eiaaf}) \\ I_{edums} &= I_{eiaaf} + G_{edums} \times I_{edums\_dlt} \end{aligned} \qquad (7)$$

where Ix_{eiaaf} and Iy_{eiaaf} are the EIAAF pre-processed neighboring horizontal and vertical pixels, respectively, of the bicubic-upscaled pixel; Sx_{ums} and Sy_{ums} represent the unsharp masking sharpening operators in the horizontal and vertical directions, respectively; G_{edums} is the manual gain used to control the edge transient performance; I_{edums_dlt} is the EDUMS processed delta; and I_{edums} is the edge-directed sharpened result, which is simulated in Figure 7c. The edges of lines at different angles are smoothly enhanced without jaggy compared to the conventional UMS method in Figure 7b.

To enhance edge clarity, this study employed pure horizontal and vertical data, which were filtered with the normalized component edge information *Edx* and *Edy*, to simulate directional data and filters without extraneous directional data and filter preparation. The ringing and jaggy issues of conventional UMS were resolved using the normalized component edge information $E_{nc}(Edx, Ei)$. The ringing effect was suppressed without degrading the details, while the jaggy effect was also reduced without using directional data or additional filters. The detail stretch and fusion processes of the EDUMS are illustrated below.

Detail fusion via edge information

After enhancing edge clarity, the detail stretch and fusion processes were performed as follows: First, the detail stretch is the main purpose of conventional UMS, which utilizes the same concept as the back projection method [15]. In a practical implementation, conventional UMS uses a high-pass filter (HPF) instead of the unsharp masking process to maintain high-frequency details. This study utilized an HPF as a detail stretch sharpening kernel (S_{dts}). Therefore, the detail stretched result I_{dts} can be modeled as follows:

$$\begin{aligned} I_{dts\_dlt} &= S_{dts} * I_{bc} \\ I_{dts} &= I_{bc} + G_{dts} \times I_{dts\_dlt} \end{aligned} \qquad (8)$$

where I_{bc} is the bicubic-upscaled source image data, I_{dts_dlt} is the detail stretch- processed delta, and G_{dts} is the manual gain used to control the detail enhancement rate.

After preparing the edge sharpened image I_{edums} and the detail sharpened image I_{dts}, the fusion process synthesized these two images according to the edge intensity *Ei*, which helped to determine the weighting of these two images. The fusion result can be modeled as

$$\begin{aligned} I' &= I_{eicl}(I_{ed} + I_{dt}) \\ let\ I_{ed} &= Ei \times I_{edums}, \quad I_{dt} = (1 - Ei) \times I_{dts} \end{aligned} \qquad (9)$$

where I_{ed} is the edge image (Figure 3d), and I_{dt} is the detail image (Figure 3e). The final output *I'* (Figure 3f) is derived from the weighted summation of I_{ed} and I_{dt}. The edge and detail enhancement rates were independently controlled by the individual gains G_{edums} and G_{dts}; stronger gains produce a more sharpened result. The blending ratio between

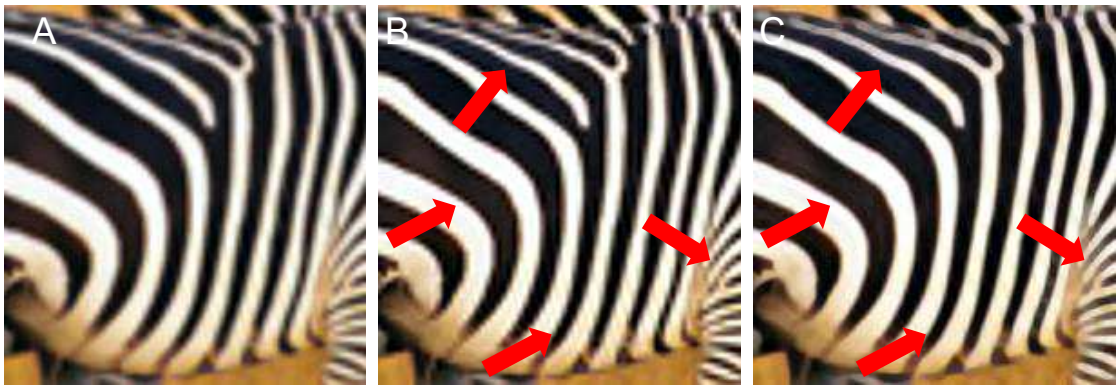

Figure 7: (a) Source image with bicubic upscaling. (b) Conventional UMS. The jaggy effect occurs for different line angles. (c) The proposed EDUMS method creates smooth and clear lines for each angle type.

these two images can be determined by the thresholds Ei_{cor} and Ei_{th}; the lower threshold produces a larger edge area. The fusion process of I_{ed} and I_{dt} enables increased flexibility in the selection of corresponding filters to enhance edges and details. The algorithm protocol of the proposed EDUMS method is shown in Algorithm 1.

Algorithm 1: *EDUMS(I)*

$I_{bc} \leftarrow Upsample(I)$

$(Edx, Ei) \leftarrow E_{nc}(I_{bc})$

$I_{eiaaf} \leftarrow I_{eiaaf}(I_{bc}, Ei)$

$I_{edums} \leftarrow I_{edums}(I_{eiaaf}, Edx)$

$I_{dts} \leftarrow I_{dts}(I_{bc})$

$I_{ed}+I_{dt} \leftarrow Fusion(I_{edums}, I_{dts}, Ei)$

$I^{\wedge}{}' \leftarrow I_{eicl}(I_{ed}+I_{dt}, I_{bc}, Ei)$

Return *I'* as the super-resolution image

Function: *Upsample(I)*

Bicubic interpolation: $I_{bc} \leftarrow I$

Return I_{bc}

Function: $E_{nc}(I_{bc})$

Normalized component gradient direction: $E_{dx} \leftarrow I_{bc}$

Edge intensity: $Ei \leftarrow Eif(m, Eicor, Eith)$

Return *(Edx, Ei)*

Function: $I_{eiaaf}(I_{bc}, Ei)$

Edge-intensity based AAF:

$I_{eiaaf} \leftarrow Ei \; x \; AAF \; {}^{*}I_{bc} + (1\text{-}Ei) \; x \; I_{bc}$

Return I_{eiaaf}

Function: $I_{edums}(I_{eiaaf}, E_{dx})$

Edge-directed UMS: $I_{edums} \leftarrow I_{eiaaf}$

Return I_{edums}

Function: $I_{dts}(I_{bc})$

Conventional UMS: $I_{dts} \leftarrow I_{bc}$

Return I_{dts}

Function: Fusion (I_{edums}, I_{dts}, Ei)

Fusion process: $I_{ed}+I_{dt} \leftarrow Ei \; x \; I_{edums} + (1\text{-}Ei) \; x \; I_{dts}$

Return $I_{ed}+I_{dt}$

Function: $I_{eicl}(I_{ed}+I_{dt}, I_{bc}, Ei)$

Edge-intensity based clipping: $I' \leftarrow I_{ed}+I_{dt}$

Return *I'*

Simulation Results and Discussion

The simulation results include A. Quantitative Evaluation and B. Qualitative Evaluation. The quantitative evaluation of image amplification includes the use of the root-mean-square (RMS), peak signal-to-noise ratio (PSNR) and structural similarity (SSIM) indexes [31]. The RMS is the root-mean-square pixel error for the evaluation of the reconstruction performance. The PSNR and SSIM are used for the evaluation of image quality and were processed by the build-in functions of Matlab R2014a. This study also compared the computational efficiency of conventional UMS, and two iterative methods, including sparse representation model (SRM) [14] and iterative Wiener filter (IWF) [16] methods. The qualitative evaluation of the visual quality compared the reconstructed image with jaggy artifact, ringing artifact, detail improvement and edge improvement. Different settings were applied to various examples to evaluate the resulting visual performance.

Quantitative evaluation

The simulation results of the evaluation of EDUMS were based on 2X magnification. The test channel consisted of a luma channel, which was processed using the EDUMS method, and a chroma channel, which was only, magnified using bicubic upscaling. This study reduced the source test images by 50% in the horizontal and vertical directions; these smaller images were used as the input *LR* image *I*. The four test images are shown in Figure 8.

In the pre-process step, the EIAAF was defined as [1, 1, 1; 1, 8, 1; 1, 1, 1]/16. According to the test conditions, this study selected sharpening operators that contained both high frequencies and middle frequencies as follows:

$$\text{EDUMS:} \quad \begin{aligned} Sx_{ums1} &= [0, -1, 2, -1, 0] \\ Sx_{ums2} &= [-1, 0, 2, 0, -1] \\ Sy_{ums1} &= [0, -1, 2, -1, 0]^{T} \\ Sy_{ums2} &= [-1, 0, 2, 0, -1]^{T} \end{aligned} \tag{10}$$

$$DT: \quad S_{dts1} = \begin{bmatrix} 0 & -1 & 0 \\ -1 & 4 & -1 \\ 0 & -1 & 0 \end{bmatrix} / 8$$

$$S_{dts2} = \begin{bmatrix} 0 & 0 & -1 & 0 & 0 \\ 0 & 0 & 0 & 0 & 0 \\ -1 & 0 & 4 & 0 & -1 \\ 0 & 0 & 0 & 0 & 0 \\ 0 & 0 & -1 & 0 & 0 \end{bmatrix} / 8$$

Figure 8: Source test images in the quantitative evaluation. (a) Lena (512 × 512 pixels). (b) Girl (768 × 512 pixels). (c) Fruits (512 × 512 pixels). (d) Monarch (768 × 512 pixels).

Here, Sx_{ums1}, Sx_{ums2}, Sy_{ums1}, Sy_{ums2}, S_{dts1} and S_{dts2} were used for the high-frequency and middle-frequency edges and details with gains of G_{edums1}, G_{edums2}, G_{dts1}, and G_{dts2}, respectively. The edge threshold and gain settings were obtained via manual fine tuning (Table 1).

The quantitative evaluation results using the RMS, PSNR and SSIM measures in the luma channel with an upscaling factor of two are listed in Table 2. Compared with the conventional bicubic and UMS methods, EDUMS produces a minimal RMS and better PSNR and SSIM values, which means the edge part of the HR images reconstructed by EDUMS have higher similarity with the original HR images. These measures do not improve significantly because the edge part actually only occupy small area of the image. However, the proposed EDUMS methods are found to be substantial better than the conventional UMS method in visual quality, as demonstrated in Figure 9. The reproduced images are discussed later (IV-B).

Additionally, this study tested the computational efficiency of the conventional UMS and proposed EDUMS methods for the luma channel. Two recently developed single-image SR methods for iterative processes, including SRM and IWF, were also compared to emphasize the difference with an upscaling factor of three because the code used by the IWF method only provides three times upscaling. The results were processed using Matlab R2014a on a computer with a 3.11 GHz CPU and 4 GB of RAM. Using the iterative methods of SRM (343608%) and IWF (184441%), the processing times are much higher than those using the conventional UMS (100%) and proposed EDUMS (177%) methods by three orders of magnitude, as shown in Table 3. Considering the processing time (computational complexity), the proposed EDUMS is found to be more promising than iterative methods for real-time IC applications, because EDUMS only added the process of edge detection and edge-directed UMS to the conventional UMS, and simultaneously enhanced the edge and detail information without artifacts. Besides, compared to conventional UMS, the EDUMS approach only increases the average computation time by approximately 80%, which remains promising for real-time applications. Most importantly, the EDUMS method produces much clearer edges and details with minimal jaggy and ringing artifacts.

ei_{cor}	ei_{th}	g_{edums1}	g_{edums2}	g_{dts1}	g_{dts2}
4	16	2.5	1.5	2.5	1.5

Table 1: Quantitative evaluation settings.

Image	method	rms	psnr	ssim
	bicubic	4.3254	35.4103	0.9304
	con. ums	5.5398	33.2609	0.9265
	edums	**4.2871**	**35.4876**	**0.9331**
	bicubic	5.8042	32.8559	0.9084
	con. ums	6.0001	32.5677	0.9163
	edums	**5.0749**	**34.0222**	**0.9179**
	bicubic	5.3841	33.5084	0.9185
	con. ums	5.9111	32.6974	0.9159
	edums	**4.6655**	**34.7529**	**0.9263**
	bicubic	5.7350	32.9602	0.9592
	con. ums	7.1431	31.0531	0.9475
	edums	**4.9625**	**34.2168**	**0.9617**

Table 2: Comparison of the super-resolution images using rms, psnr and ssim in a luma channel with an upscaling factor of two.

Image	(a)	(b)	(c)	(d)	avg.
Ir pixels	256 × 256	384 × 256	256 × 256	384 × 256	%
con. ums	0.705 sec	1.035 sec	0.672 sec	1.017 sec	100
iwf	1492 sec	1658 sec	1384 sec	1625 sec	184441
srm	2393 sec	3566 sec	2497 sec	3241 sec	343608
edums	1.243 sec	1.798 sec	1.238 sec	1.777 sec	177

Table 3: Computational efficiency of conventional ums (con. ums), iterative wiener filter (iwf) [16], sparse representation model (srm) [14], and edums with an upscaling factor of three.

Qualitative evaluation

Figure 9 compares additional upscaling images produced using the bicubic, conventional UMS, IWF, SRM and proposed EDUMS methods with three times upscaling. Compared to traditional bicubic and UMS methods, EDUMS also improved the sharpness and image details to the same level as did the iterative methods, i.e., IWF and SRM. The proposed EDUMS method properly enhanced the edge and detail area according to edge information; moreover, clipping process was applied to the edge area according to edge intensity, which prevented the detail area from blurring. The EIAAF and edge-directed UMS process prevented the jaggy artifacts, and the edge intensity-based clipping process prevented the ringing artifacts. As a result, the numbers of ringing and jaggy artifacts were substantially reduced. The simplified algorithm makes EDUMS efficient and better suited for real-time application.

This study further increased the upscaling ratio to six using EDUMS and compared the results to the nearest-neighbor method, as shown in Figure 10. The results demonstrate naturally enhanced textures and details with clear edges. Moreover, this study observed that the details were smoothly and naturally stretched by the sharpening filters. The edge structures of the images were well preserved and did not exhibit ringing and jaggy issues. The HR image styles were determined according to the enhancement ratio between the edges and the details, which were controlled by the gains of different frequency filters. By definition, EDUMS produces fine details with soft edges, soft details with strong edges or both fine details and strong edges. This study reproduced these results using a different frequency response combination, which is shown in Figures 11b-11d.

Turning to the noisy input, this study added Gaussian white noise to the low-resolution input image with a signal-to-noise ratio (SNR) of 30 dB. Compared to conventional UMS, EDUMS can still create stable and smooth edges, as shown in Figure 12. The results demonstrate that the EDUMS method is robust against noise.

Discussion

The EDUMS method was used to construct a single-image SR by synergizing edge-directed technology and the conventional UMS method. The EDUMS method minimized the ringing and jaggy issues from the two enhanced images, i.e., enhanced edge and detail images, and generated better quantitative evaluation results with substantially better visual quality compared to conventional UMS. However, comparing to conventional UMS, the processing time was increased by 80%, which was mainly resulted from the convolution process while using Sobel edge detection. Thus, further improvement of computational efficiency could be implemented by developing a much simpler way to detect the edge information. For example, using Robert's cross operators [36] instead of Sobel operators for edge detection may be a helpful choice. Robert's cross operators are 2D filters with a 2 × 2 matrix, which means it takes less time for computation while doing the convolution process in hardware implementation. However, the accuracy and fidelity of the detected edge information may be reduced and affect the quality of the reconstructed HR images. Therefore, how to make a balance between computational complexity and edge information suitability should be concerned in the future.

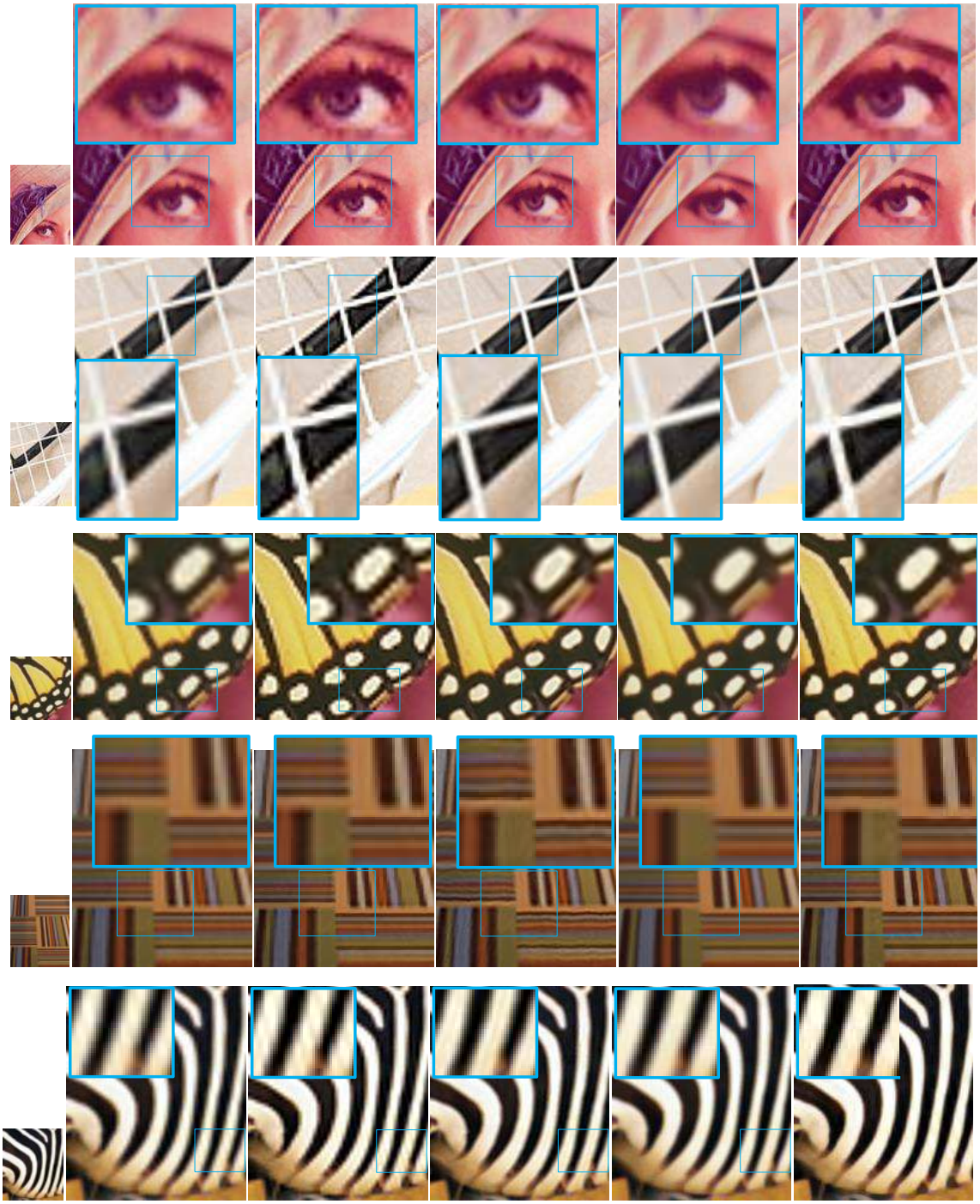

Figure 9: The 3X super-resolution results of five test images. (a) Source LR images. Processed images using (b) bicubic upscaling, (c) conventional UMS, (d) Iterative Wiener filter **Error! Reference source not found.**, (e) Sparse representation model **Error! Reference source not found.** and (f) the proposed EDUMS method.

The performance of the EDUMS method was related to the gain ratio of the filter frequency. Because the filter combination is related to the frequency characteristics of the HR images, the EDUMS approach produces a variety of results for different image quality types (Figure 11). Regardless of the filter combination type that is selected for the process, the approach is easily implemented by designers, and the artifacts are well suppressed. However, this finding generates the following questions:

First, how can suitable filters be determined for different scaling ratios? As demonstrated by our results, simple second-order differential-based filters with different frequency bandwidths constitute an effective solution. Gaussian filters are also available for general users through wiki websites or software packages (e.g., Matlab). Simple 1D filter designs, such as second-order differential-based filters, are suitable for implementation in real-time applications of filter designs. However, these filters exhibit certain basic limitations, including sharpening

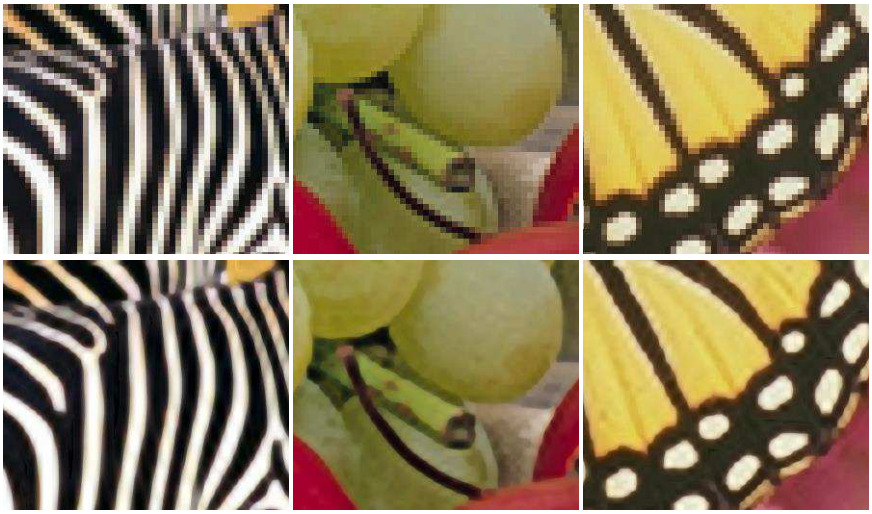

Figure 10: Resolution enhancement results with an up-sampling factor of six. The first row shows the nearest-neighbor interpolation upscaled results, and the second row shows the proposed EDUMS results.

Figure 11: The proposed EDUMS method implemented with different gain ratios. (a) Source LR image using 2X bicubic upscaling. (b) EDUMS is weak (G_{edums1}=1, G_{edums2}=2) at middle frequencies; the detail stretch (G_{dts1}=5, G_{dts2}=3) is strong at high frequencies. The results show fine details and soft edges. (c) EDUMS is strong (G_{edums1}=3, G_{edums2}=5) at middle frequencies; the detail stretch (G_{dts1}=2, G_{dts2}=1) is weak at high frequencies. The edges become clear, and the details are soft. (d) Both EDUMS (G_{edums1}=3, G_{edums2}=5) and the detail stretch (G_{dts1}=5, G_{dts2}=3) are strong. The edges and details are vivid.

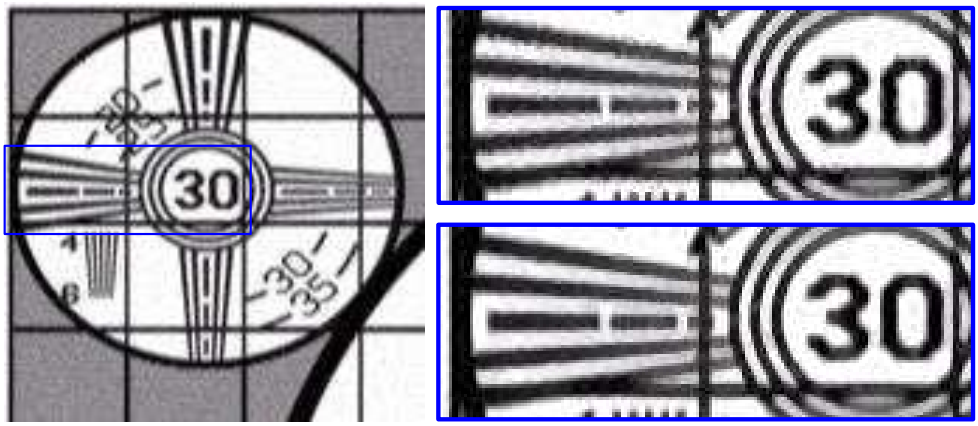

Figure 12: (a) Test image. (b) Resolution enhancement (2X) results of noisy (SNR=30 dB) low-resolution image using the conventional UMS (top) and proposed EDUMS (bottom) methods.

artifacts. To address these artifacts, the complex filter coefficient and 2D filter design may produce higher frequency details with more aliasing, which requires more complicated algorithms. With the proposed method, the simple 1D filter design becomes viable and suppresses artifacts.

Second, how can effective gain ratios for automatic edge structure similarity reconstruction be determined from LR images or reference images? Although the EDUMS method uses edge information as a generic prior for filter combination, the transient improvement rate is not determined, and no effective prior that is related to the filtering sharpening process has been developed. Manual testing for determining an optimal gain ratio can become either an advantage or a disadvantage. We believe that this requirement suggests a future direction for studies on unsharp masking sharpening SR methods. Filter designs generate edge information and more effective information that can be used to resolve the need for automatic edge structure similarity reconstruction, which is the current trend in various online studies [28-32].

Conclusion

This study proposed an efficient single-image, super-resolution method: the edge-directed unsharp masking sharpening (EDUMS) method. The EDUMS method employs edge directed sharpening to produce a clear and smooth edge structure after upscaling is performed on the low-resolution image; the details are stretched via unsharp masking sharpening from upscaled images. Using normalized component edge information, ringing from filtering sharpening was prevented, and edges jaggy from native or enhanced images were also suppressed without degrading the details. The details were accurately reproduced by stretching the upscaled image without using any other information. High-resolution image types can be intuitively and simply addressed by controlling the gain ratios of the filters' frequencies. The method preserved the advantages of unsharp masking sharpening and simplified the edge information for addressing the artifacts produced via unsharp masking sharpening. Compared to conventional UMS, the EDUMS approach increases the average computation time by only approximately 80%, which remains promising for real-time applications; however, the EDUMS method produces clearer edges and details. The proposed EDUMS method is simple and efficient and can be implemented in real-time video chip applications due to its use of a non-iterative filtering process.

Acknowledgement

The authors would like to thank Prof. Yi-Pai Huang and Prof. Han-Ping D. Shieh from NCTU, Taiwan for their valuable discussion. This study is supported by the Ministry of Science and Technology in Taiwan under the following academic project: MOST 103-2218-E-009-012.

References

1. Motohashi K (2015) The prospects of next generation television-Japan's initiative to 2020. Design Automation Conference (ASP-DAC), 677 -679, Chiba, JP.
1. James Rivington (2015) 4K TV and Ultra HD: Everything you need to know. TechRadar.
2. Farsiu S, Dirk R, Michael E, Peyman M (2004) Advances and challenges in superresolution. Int J Imag Syst Technol 14: 47-57.
3. Van Ouwerkerk JD (2006) Image super-resolution survey. Imag Vis Comput 24: 1039-1052.
4. Atkins CB, Bouman CA, Allebach JP (1999) Tree-based resolution synthesis. Proc Conf Image Processing, Image Quality, Image Capture Systems 405-410.
5. Atkins CB, Bouman CA, Allebach JP (2001) Optimal image scaling using pixel classification. Proc ICIP 3: 864-867.
6. Chang H, Yeung DY, Xiong Y (2004) Super-resolution through neighbor embedding. Proc IEEE Conf Comput Vis Pattern Recognit 3: 275-282.
7. Ni KS, Nguyen TQ (2007) Image superresolution using support vector regression. IEEE Trans Image Process 16: 1596-1610.
8. Glasner D, Shai Bagon, Michal Irani (2009) Super-resolution from a single image. Proc IEEE Int Conf Comput Vis 349-356.
9. He H, Siu WC (2011) Single image super-resolution using Gaussian process regression. Proc IEEE Conf Comput Vis Pattern Recognit 449-456.
10. Yang, Wright J, Huang T, Yi Ma (2008) Image super-resolution as sparse representation of raw image patches. Proc IEEE Conf Comput Vis Pattern Recognit 1-8.
11. Kim KI, Kwon Y (2010) Single-image super-resolution using sparse regression and natural image prior. IEEE Trans Pattern Anal Mach Intell 32: 1127-1133.
12. Mallat S, Yu G (2010) Super-resolution with sparse mixing estimators. IEEE Trans Image Process 19: 2889-2900.
13. Dong W, Lei Zhang, Lukac R, Guangming Shi (2013) Sparse Representation based Image Interpolation with Nonlocal Autoregressive Modeling, IEEE Trans Image Process 22: 1382-1394.
14. Dai SY, Mei Han, Ying Wu, Yihong Gong (2007) Bilateral back-projection for single image super resolution. Proc IEEE Conf Multimedia and Expo 1039-1042.
15. Hung KW, Siu WC (2012) Single image super-resolution using iterative Wiener filter. Proc IEEE Conf Acoustics, Speech and Signal Processing (ICASSP) 1269-1272.
16. Polesel A, Ramponi G, Mathews VJ (2000) Image enhancement via adaptive unsharp masking. IEEE Trans Image Process 9: 505-510.
17. Dnyaneshwar V, Haralkar S, Kanade Sudhir (2013) Performance and Analysis of Improved Unsharp Masking Algorithm for Image Enhancement. International Journal of Electronics in press.
18. Aditya, Meher S (2012) An efficient, adaptive unsharp masking based interpolation for video intra frame up-sampling. Proc IEEE Asia Pacific Conference on Postgraduate Research in Microelectronics and Electronics 100-105.
19. Deng G (2011) A generalized unsharp masking algorithm. IEEE Trans Image Process 20: 1249-1261.
20. Ramponi G, Norbert KS, Sanjit KM, Tian-Hu Yu (1996) Nonlinear unsharp masking methods for image contrast enhancement. Journal of Electronic Imaging 5: 353-366.
21. Cao G, Zhao Y, Rongrong Ni (2009) Detection of image sharpening based on histogram aberration and ringing artifacts. Proc IEEE Conf Multimedia and Expo, ICME 1026-1029.
22. Fischer M, Paredes JL, Arce GR (2002) Weighted median image sharpeners for the World Wide Web. IEEE Trans Image Process 11: 717-727.
23. Lukac R, Smolka B, Plataniotis KN (2007) Sharpening vector median filters. Signal Process 87: 2085-2099.
24. Raju R, Hemachandran K (2011) A Review on Image enhancement of fingerprint using Directional filters. Assam University Journal of Science and Technology 7: 52-57.
25. Zhang L, Wu X (2006) An edge-guided image interpolation algorithm via directional filtering and data fusion. IEEE Trans Image Process 15: 2226-2238.
26. Pelletier S, Cooperstock JR (2012) Preconditioning for edge-preserving image super resolution. IEEE Trans Image Process 21: 67-79.
27. Jiji CV, Chaudhuri S (2006) Single-frame image super-resolution through contourlet learning. EURASIP Journal on Applied Signal Processing 235.
28. Tai YW, Tong WS, Tang CK (2006) Perceptually-inspired and edge-directed color image super-resolution. Proc IEEE Conf Comput Vis Pattern Recognit 1948-1955.
29. Sun J, Xu Z, Shum HY (2011) Gradient profile prior and its applications in image super-resolution and enhancement. IEEE Trans Image Process 20: 1529-1542.
30. Wang Z, Alan CB, Hamid RS, Eero PS (2004) Quality assessment: From error measurement to structural similarity. IEEE Trans Pattern Anal Mach Intell 13: 600-612.

31. Cho TS, Zitnick CL, Joshi N, Kang SB, Szeliski R, et al. (2012) Image restoration by matching gradient distributions. IEEE Trans Pattern Anal Mach Intell 34: 683-694.

32. Yu LC, Hongteng Xu, Yi Xu, Xiaokang Yang (2012) Robust single image super-resolution based on gradient enhancement. IEEE Signal and Information Processing Association Annual Summit and Conference (APSIPA ASC) 1-6.

33. YW Tai, Shuaicheng Liu, Brown MS, Lin S (2010) Super resolution using edge prior and single image detail synthesis. Proc IEEE Conf Comput Vis Pattern Recognit 2400-2407.

34. Canny J (1986) A computational approach to edge detection. IEEE Trans Pattern Anal Mach Intell 8: 679-698.

35. Maini R, Aggarwal H (2009) Study and Comparison of Various Image Edge Detection Techniques. International Journal of Image Processing 3: 1-11.